

Supporting Information

Toward advanced sodium-ion batteries: a wheel-inspired yolk-shell design for large-volume-change anode materials

Hui Xu¹, Liguang Qin¹, Jian Chen^{1*}, Zuankai Wang^{2*}, Wei Zhang¹, Peigen Zhang¹, Wubian Tian¹, Yao Zhang¹, Xinli Guo¹, Zhengming Sun^{1*}

1 Jiangsu Key Laboratory of Advanced Metallic Materials, School of Materials Science and Engineering, Southeast University, Nanjing 211189, China

2 Department of Mechanical and Biomedical Engineering City University of Hong Kong, Hong Kong 999077, China

*E-mail: j.chen@seu.edu.cn; zuanwang@cityu.edu.hk; zmsun@seu.edu.cn

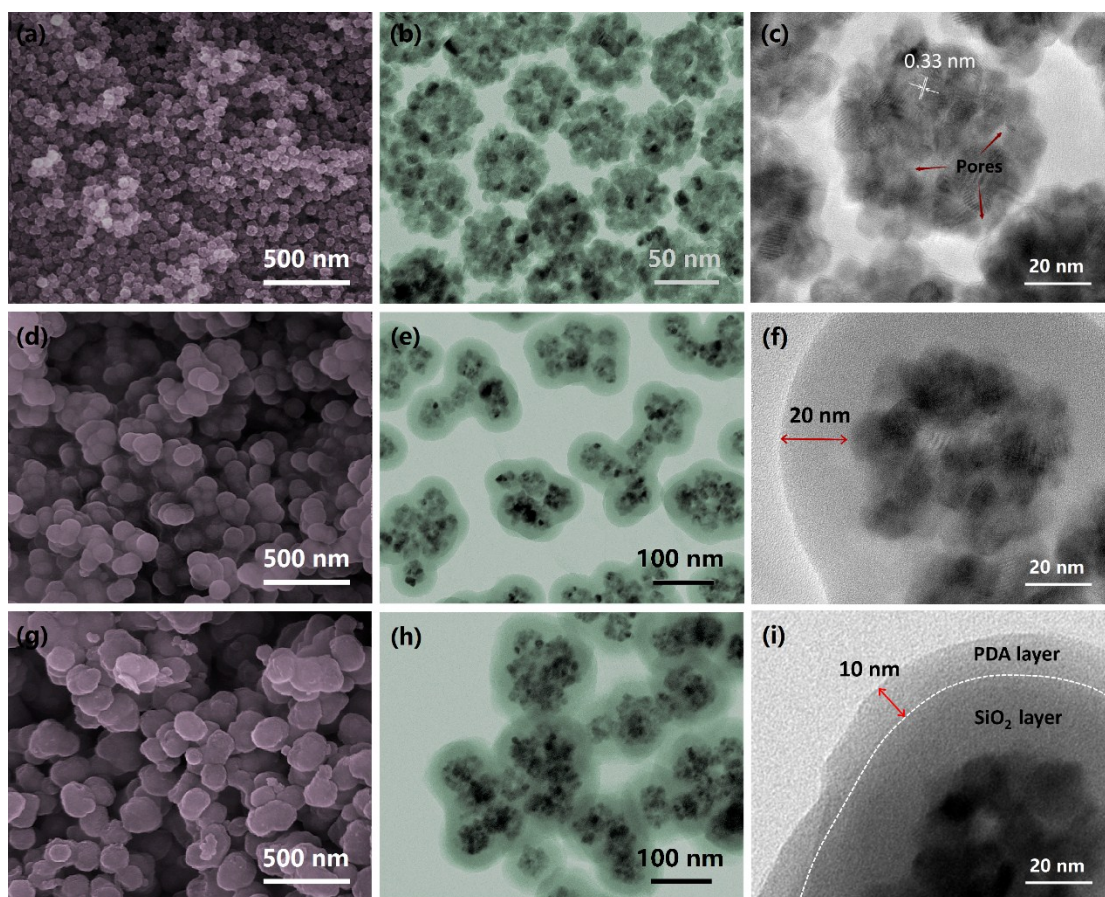


Figure S1. (a) SEM image and (b, c) TEM images of P-SnO₂ NSs, (d) SEM image and (e, f) TEM images of SnO₂@SiO₂ particles, (g) SEM image and (h, i) TEM images of SSP particles.



Figure S2. Photographs image of SSP@GO foam monoliths.

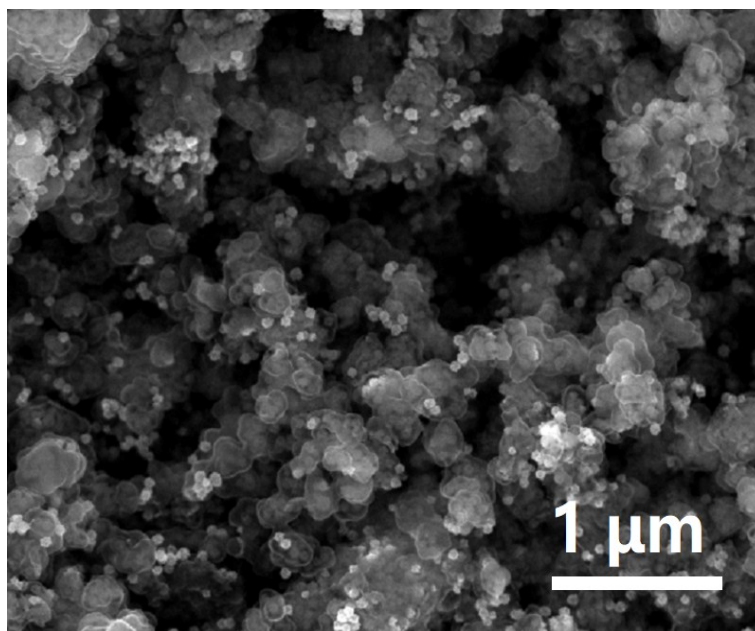


Figure S3. SEM image of YS with NaOH as etching agent. Some exposed P-SnO₂ NSs can be clearly seen outside the carbon shells.

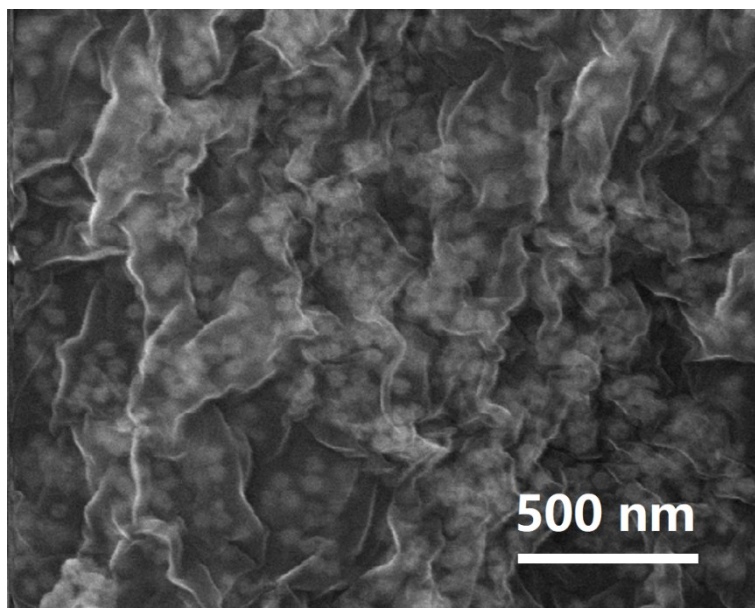


Figure S4. High-magnification SEM image of WS structure.

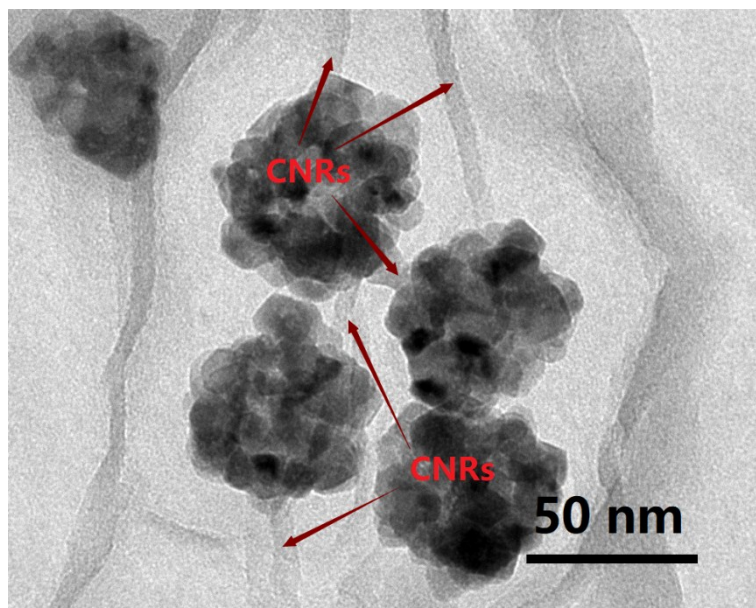


Figure S5. TEM image of WS structure.

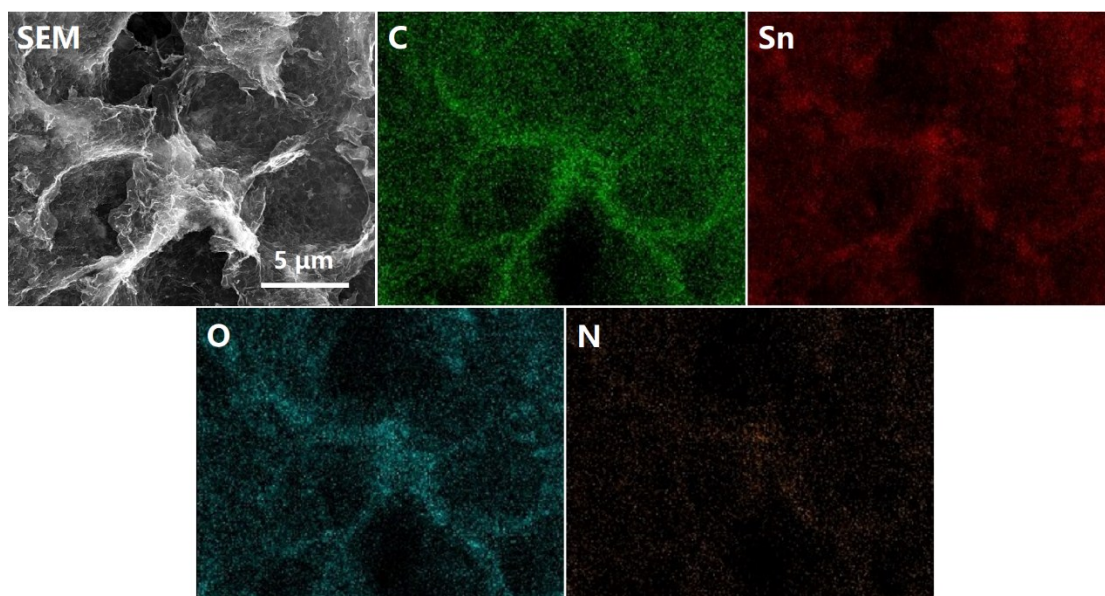


Figure S6. SEM image and the corresponding elemental mapping images of WS.

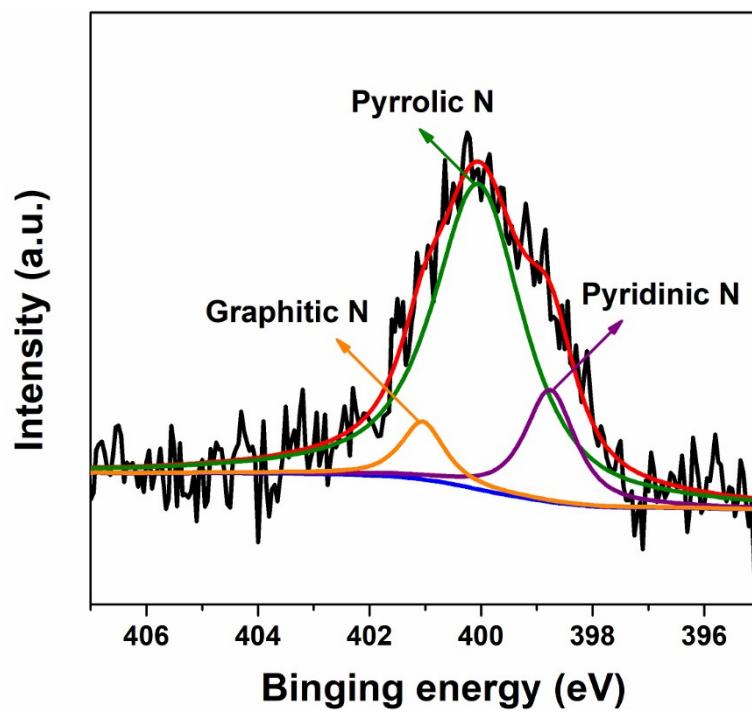


Figure S7. XPS spectrum of N1s for WS.

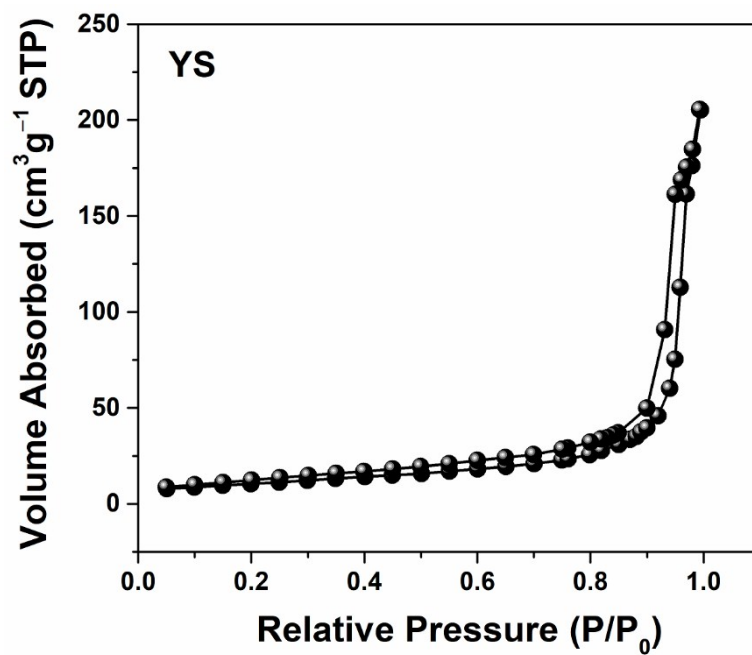


Figure S8. Nitrogen adsorption-desorption isotherms of YS.

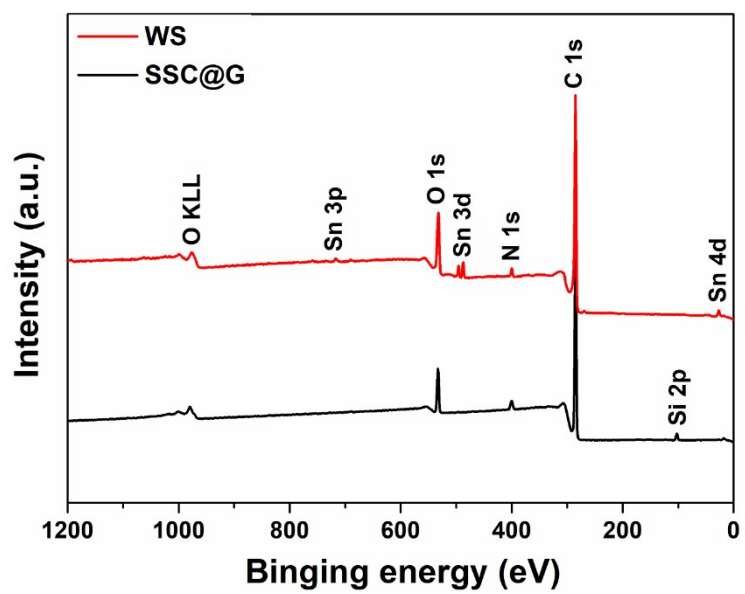


Figure S9. Survey XPS spectra of SSC@G and WS.

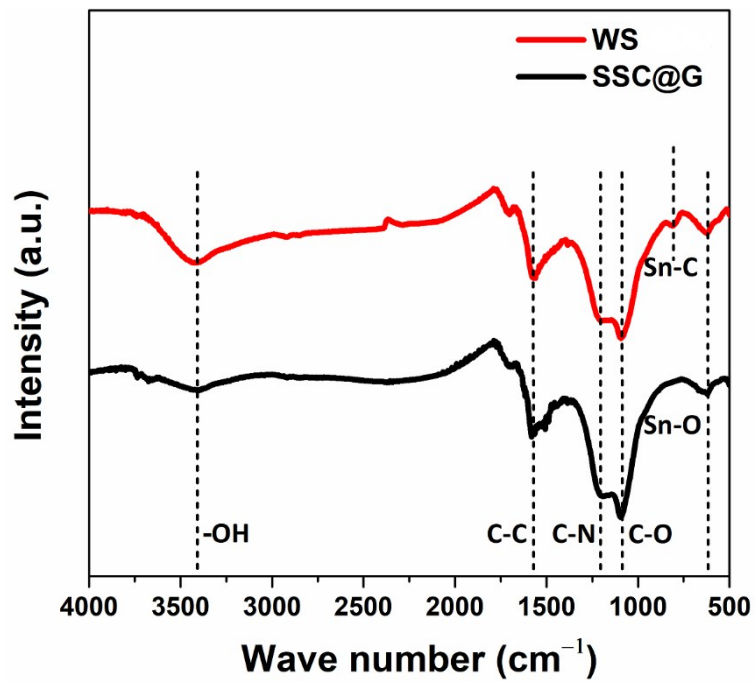


Figure S10. FTIR spectra of SSC@G and WS.

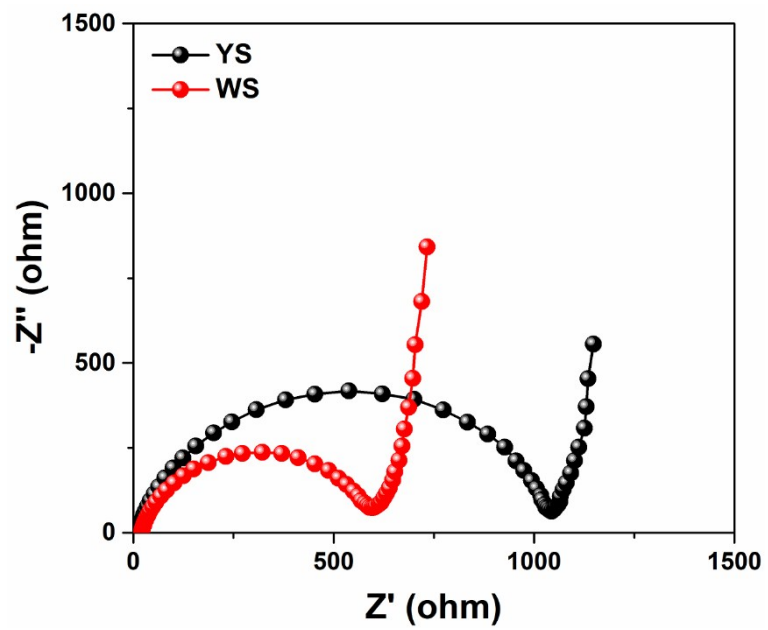


Figure S11. EIS of WS and YS electrodes.

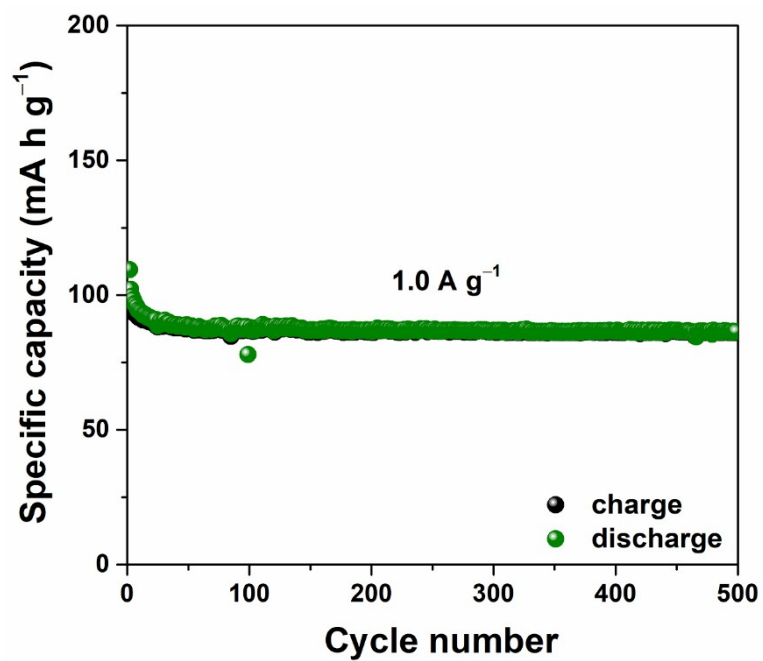


Figure S12. Cycle performance of pure graphene at a current density of 1.0 A g^{-1} .

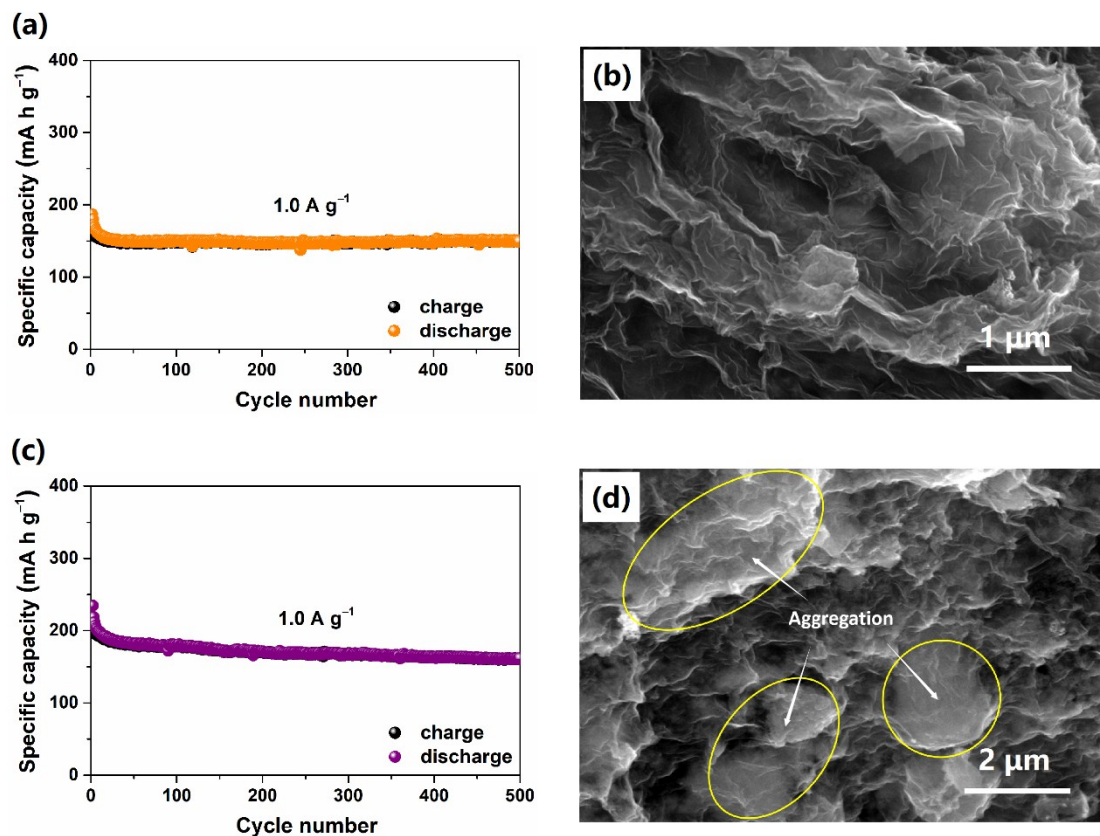


Figure S13. Cycle performance at 1.0 A g^{-1} and SEM images of (a, b) the sample with a lower SnO_2 amount, and (c, d) the sample with a higher SnO_2 amount.

The samples with both lower and higher SnO_2 loading amount were prepared by changing the ratio of SSP/GO to 1:2 and 2: 1 in the precursor suspensions, respectively. Compared with the WS (SSP/GO is 1:1), the sample with a lower SnO_2 amount only maintains a low reversible capacity of $149.5 \text{ mA h g}^{-1}$ after 500 cycles (Figure S13a), which is ascribed to its relative lower SnO_2 amount. The SEM result (Figure S13b) also demonstrates an inadequate SnO_2 encapsulation amount in this sample. Whereas the sample with a higher SnO_2 amount not only delivers a low reversible capacity of $161.6 \text{ mA h g}^{-1}$ after total 500 cycles, but also exhibits a noticeable capacity fading upon cycling (Figure S13c). This can be attributed to the severe aggregation of the P- SnO_2 NSs in this sample (Figure S13d), which caused difficulties for efficient Na^+ diffusion, leading to part of the active materials inaccessible to Na^+ .

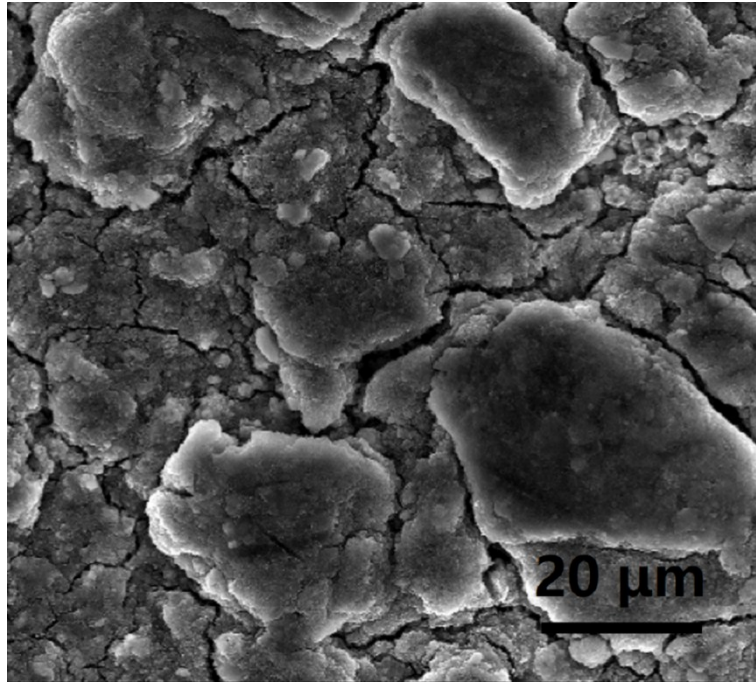


Figure 14. SEM image of YS electrode after 100 cycles.

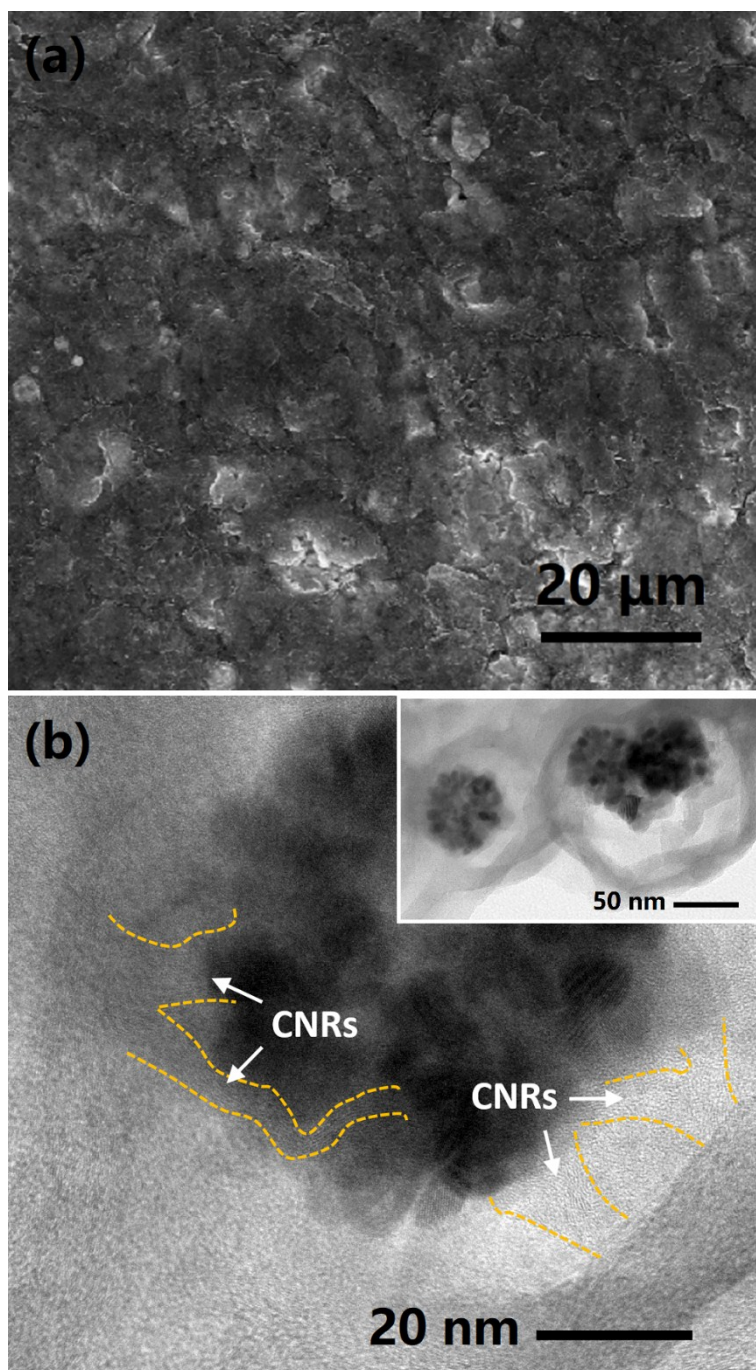


Figure S15. (a) SEM image and (b) TEM image of WS electrode after 100 cycles.

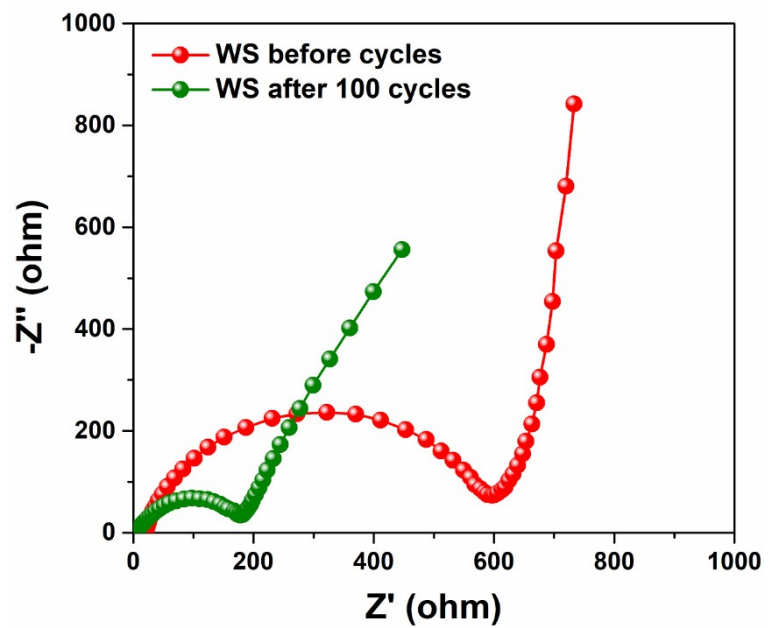


Figure S16. EIS of WS electrode before and after cycles.

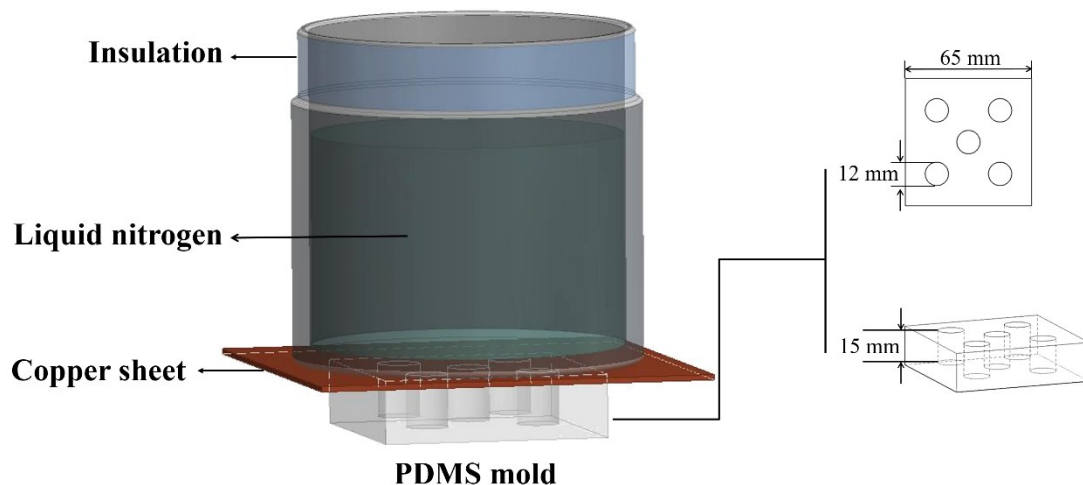


Figure S17. Schematic illustration of the freeze-casting equipment.

The freeze-casting equipment used in this study is designed by ourselves, and each of its components is schematically shown in Figure S17. The polydimethylsiloxane (PDMS) mold is made by a casting molding process. In brief, several ceramic cylinders with diameter of 12 mm and height of 15 mm were placed into a square groove with side length of 65 mm and depth of 30 mm. The PDMS mixture was stirred and then slowly poured into the groove until the top of the cylinders was submerged. Subsequently, this groove was placed under vacuum to get rid of the bubbles in the PDMS and then be dried overnight.